# The impact of Platelet Rich Plasma (PRP) in osseointegration of oral implants in dental panoramic radiography: texture based evaluation

**Ioannis Georgakopoulos[1]**
**Stavros Tsantis[2]**
**Panagiotis Georgakopoulos[3]**
**Panagiotis Korfiatis[4]**
**Elena Fanti[5]**
**Marialaura Martelli[5]**
**Lena Costaridou[4]**
**Theodoros Petsas[1]**
**George Panayiotakis[4]**
**Francesco Saverio Martelli[5]**

[1] Department of Radiology, School of Medicine, University of Patras, Patras, Greece
[2] Department of Medical Instrumentation Technology Technological Educational Institution of Athens, Egaleo, Athens, Greece
[3] University Alfonso X El Sabio, School of Dentistry, Madrid, Spain
[4] Department of Medical Physics, School of Medicine, University of Patras, Patras, Greece
[5] IRF in Microdentistry, Florence, Italy

Author for correspondence:
Ioannis Georgakopoulos
Department of Radiology, School of Medicine
University of Patras, 265 00 Patras, Greece
Akademias str. Athens 106 72, Greece
Phone: +30 2103624881
Fax: +30 2103600122
E-mail: ioangeo@upatras.gr, dentisteduipg@gmail.com

**Summary**

***Purpose*. In this study the temporal texture differentiation associated with the bone formation properties, around loaded oral implants after Platelet Rich Plasma (PRP) employment, was investigated in Panoramic Radiographs.**
***Materials and methods*. Thirty eligible patients are randomly assigned to two groups. The test group received PRP application around new implants, while in the control group no PRP treatment was made. The bone-to-implant contact region was analyzed in a clinical sample of 60 Digitized Panoramic Radiographs, 30 corresponding to immediate implant loading (Class-I) and 30 after an 8 month follow-up period (Class-II). This region was sampled by 1146 circular Regions-of-Interest (ROIs), resulting from a specifically designed segmentation scheme based on Markov-Random-Fields (MRF). From each ROI, 41 textural features were extracted, then reduced to a subset of 4 features due to redundancy and employed as input to Receiver-Operating-Characteristic (ROC) analysis, to assess the textural differentiation between two classes.**
***Results*. The selected subset, achieved Area-Under-Curve (AUC) values ranging from 0.77-0.81 in the PRP group, indicating the significant temporal textural differentiation has been made. In the control group, the AUC values ranged from 0.56-0.68 demonstrating lesser osseo integration activity.**
***Conclusion*. This study provides evidences that PRP application may favor bone formation around loaded dental implants that could modify the dental treatment planning.**

*KEY WORDS: Platelet Rich Plasma; dental implants; medical image texture analysis; implant segmentation; Markov Random Fields; radiography.*

## Introduction

Implantology has been the key factor in dentistry effectiveness throughout the last few decades. Although a number of restorative options for the treatment of missing teeth still exist, none have proven to be as functionally effective and robust as implants. In many cases, dental implants may be the only consistent and successive choice for the restoration of all necessary functionality of the teeth and supporting structures. The majority of dental implants in use today are made from titanium or titanium alloy (1). Studies have shown a five-year success rate of 95% for lower jaw implants and a 90% success rate for upper jaw implants. The success rate for upper jaw implants is slightly lower because the upper jaw (especially the posterior section) is less dense than the lower jaw, making a successful implantation and osseointegration potentially more difficult to achieve (2).
Despite the high success rate of dental implants, the osteo-regenerative potential of the surrounding tissues (soft and hard) that substantially affect the outcome of the overall surgical procedure still remains an important issue. Several studies have shown that the surgical placement of implants in sites with poor osteo-regenerative properties has a decreased probability of success. A high degree of primary implant stability (high value of insertion torque) seems to be one of the prerequisites for a successful procedure (2). Dental implants may break or become infected (like natural teeth) and crowns may become loose. In order to promote healing of end-osseous implants and bone grafts, various procedures have been proposed. The majority of these proposals concentrate on strengthening the bone-to-implant contact area so as to accelerate the osseous healing. These, include the application of Platelet Rich Plasma (PRP), bone morphogenetic proteins (BMPs) and growth factors (3).
Platelet Rich Plasma is an autologous concentration of human platelets in a small volume of plasma. Due to its concentration of platelets, PRP consists of the 7 fundamental protein growth factors proved to be actively secreted by platelets. These growth factors include the three isomeres of

platelet-derived growth factor (PDGFαα, PDGFββ, and PDGFαβ), two of the numerous transforming growth factors-β (TGFβ1 and TGFβ2), vascular endothelial growth factor, and an epithelial growth factor. All the aforementioned growth factors possess anti-inflammatory and pro-regenerative properties that permit tissue wounds to heal faster and more efficiently. Additionally they can stimulate cell proliferation, matrix remodeling and angiogenesis (4, 5).

The use of these growth factors in order to enhance healing is of a great interest to a large number of researchers and clinicians. Their main approach is the PRP effect in bone regeneration analyzing histological and histomorphometric data of animal and human tissue. The majority of these studies report a significant enhancement of healing when PRP is used with positive results in either or both bone and soft tissue healing. In these studies an enhancement of bone regeneration is also observed (6-8).

However, in disagreement with most of scientific evidences, there have also been authors supporting the hypothesis that there was little or no benefit from PRP treatment (9, 10). The results of these studies could be affected by the design of the experiment or by the too short follow-up period that has not allowed to appreciate the real differences in new bone formation induced by the addition of PRP.

The commercial exploitation of these growth factors has led to the development of a wide range of preparation protocols, kits and centrifuges. Most of these products were called PRP, the same name as the original transfusion platelet concentrates, which does not allow distinction between the different systems and protocols employed (11, 12). Only a few studies have attempted to quantify dental bone density and the PRP effect in dental implantations (13-17). Gatti et al. (13) investigated the bone density alteration, based on the gray level values, around the implant in three different types of dental implants which were placed in dogs. Youssif et al. (14) presented a new approach of applying computer algorithms to radiographic images of dental bone implantation used for bone regeneration. This study is applied to two dental cases at different follow up times so as to assess the rate of bone density alterations by comparing the baseline radiograph to the follow up images. The density changes at the intra-bony affected area are assessed by means of a statistical analysis of parameters from the gray-level histogram and have shown a 37.32% and a 63.37% increase in the bone density by the end of the follow up period of about 12 months.

Barone et al. (15) analyzed the bone density around the loaded oral implants by using a new volumetric CT scan and compared it to unloaded implants. Four patients were selected for this study. A total of 12 oral implants were placed. In these patients six of these implants were loaded immediately, while six were left unloaded. Six months after the placement of immediately loaded and unloaded oral implants, they were analyzed by a volumetric CT scan by means of the densitometric profile from para-axial slices (mean and standard deviation values). The differences observed between the two groups of the oral implants (immediately loaded and unloaded) were statistically significant ($p<0.05$).

Wilding et al. (16) also investigated the possibility that fractal dimensions of bone images taken from routine orthopantomograms could be used to observe and to monitor bone remodelling in response to dental implants. This study involved 18 patients who had received fixed implant-supported prostheses. A window of bone adjacent and distal to the most posterior implant was defined as the region of interest from which the fractal dimension of the image was calculated in order to evaluate whether there were any significant shifts in fractal dimension during the recall period after implantation. A significant increase in fractal dimension was found during the period up to 2 years after implantation ($p < 0.001$).

Wojtowicza et al. (17) studied the regeneration of the maxillary alveolar process after PRP use in a 17-year-old patient who had lost the upper central incisors together with the alveolar bone as a result of a car accident. The regenerated bone was analyzed after 10 months and compared to the intact bone using the Fourier and fractal analysis of radiograms. Fractal analysis of intact and regenerated bone showed a higher fractal dimension for the intact bone in comparison with the regenerated bone, confirming a lower complexity of the newly formed trabecular structures.

For the first time a randomized experimental case control study, in terms of a computerized texture analysis, of platelet-rich plasma (PRP) as a promoter of bone healing in dental implants is carried out. The main objective was to quantify any texture differentiation that occurred during the 8 month follow up period, into the bone-to-implant contact region, between the two classes (0 & 8 month follow up period) and consequently to evaluate any statistical difference between test and control groups that can be attributed to the PRP treatment. The texture analysis in association with bone formation properties around the loaded oral implants was employed in the panoramic radiographs by means of first order, co-occurrence, run length textural features and Receiver Operating Characteristic (ROC) curve analysis.

## Materials and methods

### *Clinical dataset and surgical procedures*

This study has undergone an ethics review by the University of Patras Ethics Board. A clinical dataset of 30 patients was selected for the study that was randomly assigned to two groups (test group-15 patients, control group-15 patients). Ages within the clinical dataset ranged from 25-65 years. Exclusion criteria for participating in to the study were mainly diabetes, osteoporosis, cardiac and thoracic diseases, non-smoking and cancerous patients. All patients that were finally chosen had maxillary and mandibular tooth loss and had chosen the surgical implant solution although they had been advised of an alternative treatment plan such as prosthetics. They had all been informed of the requirements for participation in the study and had a consent form signed. The test group received the PRP application around new implants and within the surgical site whereas in the control group the new implants were placed without PRP treatment. A follow up clinical sample of 60 digitized panoramic radiographs, corresponding to the 30 patients imaged immediately after implant loading (Class I) and 8 months later (Class II) were analyzed.

All surgical procedures were performed under local anesthesia (Ubistesin forte - 1.7 ml). A number of 2 - 6 implants were placed in each patient. The bone surface was exposed by of type -H- Incision. Bone defects of 3.60 mm were created. Implants 11.50 mm in length and 3.75 mm in diameter were then placed (MF7-11375, MIS Implants Technologies Ltd, Israel) after been immersed in PRP. PRP was also placed within each surgical site before implant loading.

PRP was derived in the test group with the following procedure: a 40 ml of autologous blood was drawn from each pa-

tient the sample initially centrifuged at 2400 rpm for 10 min in order to separate the PRP and the platelet-poor plasma (PPP) from the red blood cells. Following both the PRP and PPP were again centrifuged at 3600 rpm for 15 min to further separate the PRP from the PPP. Platelet counts were then done for each patient. Subsequently, the PRP was activated just before application with a 10% calcium chloride solution (18).

An image dataset consisting of two panoramic radiographs for both groups, the first one (Class I, 76 implants) was acquired immediately after surgery (baseline panoramic radiograph) and the second one (Class II, 76 implants), eight months later (19) leading to a total of 60 radiographs, is analyzed. All (baseline) radiographs had a one-to-one correlation to those obtained after the 8 month follow up period.

Regarding the standardization of the panoramic radiographs all images were taken by the same technician according to a standardized protocol for patient positioning and exposure parameter setting. In addition, in for each patient a registration method (Matlab built-in intensity based algorithm that employed as input the output from the MRF-based segmentation method introduced in this study) utilized the mean square error metric derived from the segmented implants in order to compensate any minor geometrical misalignment between the two panoramic radiographs of each patient (0 & 8 months). The majority of the images (baseline and follow up) produced a mean square error close to zero. As a result, all (baseline) radiographs had a one-to-one geometrical correlation to those obtained after the 8 month period.

The follow up period is within the time range of (6 to 12 months) as already proposed in most of the aforementioned studies (clinical and quantitative) and has been considered adequate for bone regeneration evaluation by the expert dentist participated in this study. Figure 1 highlights the region from an implant in which the texture analysis has been employed along with relevant zoomed area indicating a radiological appearance of the patterns that were considered.

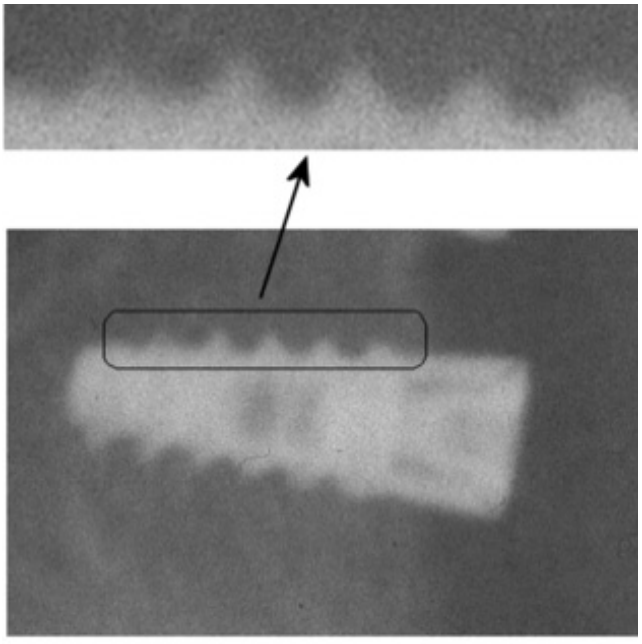

Figure 1 - Oral implant of a dental panoramic radiograph. Zoomed image part at arrow locations indicate the bone-to-implant regions in which the texture analysis is applied. The differentiations in radiologic appearance patterns (increased gray tone illumination and variability) of the bone-to-implant area are been considered towards efficient segmentation.

The panoramic x-ray equipment that utilized was the Orthophos C (Siemens co, AG Wittelsbacherplatz 2, 80333 Munich, Germany) and the radiographic parameters were set at 66-69 kVp and 16 mA. All panoramic radiographs were digitized by the MicrotekScanMaker i800 (Positive film, 600 dpi, 16 bit grayscale) scanner (Microtec Industries, Silicon valley, Taiwan). The software employed for digitization and storage was the MicrotekScanwizard Pro V7.11. The provided digitized images were in TIFF format (Tagged-Image File Format). The x-ray equipment as well as the film digitizer performance were evaluated, employing appropriate quality control protocols, so as to ensure proper functioning of the medical equipment and the high quality of the digitized images (20, 21).

***Identification of bone-to-implant contact region (ROIs)***

A specifically designed detection algorithm was targeted to identify ROIs from panoramic radiographs so as to sample the bone to implant contact region. This region encompasses tissue in between and adjacent to implant windings, candidate for bone regeneration. Accurate ROI identification is critical, as over-segmentation (inclusion of an implant border) or under-segmentation (loss of valuable information within the implant's windings) would compromise subsequent texture analysis.

At first, the dental implant is extracted from the surrounding tissue by means of the Markov Random Field (MRF) method (22). MRF modeling combines conditional (local intensity distribution) with contextual (intensity similarity within small neighborhoods) information under the Bayesian framework in order to estimate the true intensities of the image rather than those based only on the conditional information (23). It assumes that the class probability of a pixel is only dependent on class membership of its spatial neighbors (also called lattice) which in turn reduces the possible influence of noise and overlapping structures. The model assumption that the conditional distribution depends on the pixels in the near neighborhood is subject to the Bayesian framework which states that the decision rule for labeling an image pixel combines the conditional intensity distribution of an individual region with prior knowledge regarding that region.

Let us assume that *P(X)* is our prior knowledge and *P(Y|X)* is the probability of realizing the observed image given the distribution of regions in the image. The most widely used conditional intensity distribution is the Gaussian distribution, whose function, given the class $x_s$ is given by:

$$P(Y = y \mid X = x_s) = \frac{1}{\sqrt{2\pi\sigma_s^2}} e^{\frac{(y-\mu_s)^2}{\sigma_s^2}} \qquad (1)$$

where $\mu_s$ and $\sigma_s$ are the parameters of the distribution of the class $x_s$.

Then, by Bayes' theorem

$$P(X \mid Y) = \frac{P(Y \mid X)P(X)}{P(Y)} \qquad (2)$$

where *P(X|Y)* is our posterior.

Then $\hat{x}$ can be obtained by taking the negative of the posteriori estimate natural logarithm and minimizing it[18]:

$$\hat{x} = \arg\min_x(-\log(P(X \mid Y))) \qquad (3)$$

Simulated annealing and iterated conditional modes are the two main approaches in order to solve the optimization problem. In this study the stochastic approach, simulated annealing (SA) was implemented (24).
The SA solves the minimization problem by sequentially updating (i.e raster scanning the image) labels by minimizing the following equation at each pixel s:

$$\hat{x} = argmin_{x_s \in L} = \left\{ \frac{(y - \mu_s)}{\sigma_s^2} + \frac{1}{2} log(2\pi\sigma_s^2) + \beta U(x_s) \right\} (4)$$

where $U(x_s)$ is the number of pixels in the neighborhood that have the color $x_s$.
After the dental implant boundary extraction, the particular interface region (i.e. tissue in between and adjacent to the implant windings) in the binary images was sampled by circular Regions Of Interest (ROIs) that were derived from the specifically designed detection method based in morphological closing by means of circular closing elements of varying size. Finally, two ROI classes for both groups were created corresponding to the radiographs acquired immediately after the implant and 8 months later.

### *Texture and statistical analysis*

Forty-one (41) textural features were automatically calculated from each segmented ROI. The textural features are related to the gray-tone structure for the bone-to-implant interface and possess information relevant to the osseo-integration potential in that region. Four (4) features were computed from the gray-tone histogram, while the mean and range of Thirteen (13) second order statistic features, extracted from the co-occurrence matrices and Five (5) features extracted from the run-length matrices over four directions ($0^0$ , $45^0$, $90^0$ and $135^0$) and a distance of $d$=1 pixel, resulting in 26 and 10 features respectively (25, 26). Additionally, the fractal dimension feature was also computed carrying information regarding the degree of gray level complexity (Table 1) (27). The selected feature set, provides significant information, regarding the evaluation of a possible change throughout the 8 month period of spatial and intensity dependencies of the pixels within the bone-to-implant region that can be attributed to the osseo-regeneration procedure. Moreover, the generated features must encode this kind of information in order exhibit high separability attributes between the two classes.
Ideally, all 41 features at hand should be utilized, but since a number of them may be redundant due to mutual correlations, an optimum number of them had to be selected to achieve the highest discrimination. A common technique in achieving this is the Stepwise Regression Analysis (SRA) that led to a subset of features that is significant different and carries the aforementioned discriminant properties (28). SRA is a sequential feature selection technique specifically designed for least-squares fitting in a multiple regression model. It is based on an add/remove features scheme from a multilinear model based on their statistical significance in a regression. The stepwise regression procedure starts off by choosing an equation containing the single best feature and then attempts to build up with subsequent additions of other features one by one as long as these features are 'statistically significant' or highly correlated with that feature.

Table 1 - Textural features employed in the texture-based evaluation of bone formation properties of PRP.

| | Textural Feature |
|---|---|
| | **Gray-Tone Histogram Features** |
| 1 | Mean value (m) |
| 2 | Standard Deviation (std) |
| 3 | Skewness (sk) |
| 4 | Kurtosis (k) |
| | **Co-Occurrence Features** |
| 5 | Angular Second Moment (ASM) |
| 6 | Contrast (CON) |
| 7 | Inverse Different Moment (IDM) |
| 8 | Entropy(ENT) |
| 9 | Correlation(COR) |
| 10 | Sum of Squares (SSQ) |
| 11 | Sum Average (SAV) |
| 12 | Sum Entropy (SENT) |
| 13 | Sum Variance (SVAR) |
| 14 | Difference Variance (DVAR) |
| 14 | Different Entropy (DENT) |
| 16 | Information Measure of Correlation (ICM1) |
| 17 | Information Measure of Correlation (ICM2) |
| | **Run-Length Features** |
| 18 | Short Run Emphasis(SRE) |
| 19 | Long Run Emphasis(LRE) |
| 20 | Grey Level Non Uniformity (GLNU) |
| 21 | Run Length Non Uniformity (RLNU) |
| 22 | Run Percentage (RP) |
| 23 | Fractal Dimension (FD) |

The order of addition is determined by using the partial F-test values in order to select which feature should enter next. The highest partial F-value is compared to a selected F-to-enter value. A feature is considered significant and is added provided that its highest partial F-value is less to the selected F-to-enter value. After a feature is added, the regression equation is examined to see if any feature already added in the earlier stages of the procedure should be removed because of the relationship between it and other new added variables now in the regression model. A feature is removed if its highest partial F-value is greater than the selected F-to-remove value. Stepwise regression has the advantage of removing features that have been added or adding features that have been removed during the regression process and follows the "minimum redundancy - maximum relevance" principle as adopted by several recently proposed feature selection methods (29). The filter-based approaches for feature selection such as SRA provide the identification of the discriminant features, instead of the so called wrapper ap-

proaches such us Principal Component Analysis (PCA) which can only estimate a good feature subset (30).

Statistical differentiation for the selected subset was exploited by means of ROC curve analysis. The ROC curve is a plot of the true positive rate (sensitivity) versus the false positive rate (1-specificity) for different thresholds over the entire range of each feature values and it is independent of class distribution or error costs. The AUC can be statistically interpreted as the probability that a random (class I, Class II) pair of feature values will be correctly discriminated (31). ROC analysis has been utilized to assess the discriminant power of each independent feature from the selected subset. Features achieving the highest Area Under the Curve (AUC) are capable of capturing the osseo integration enhancement due to the PRP employment. The AUC values were obtained by the binormal parametric method in order to approximate the area (31). It computes the AUC by fitting two normal distributions to the data. Compared to the empirical ROC approach, the binormal ROC is computationally more affordable and robust in small sample size cases (32).

Prior to calculation of textural features, normalization in each ROI was implemented so as to compensate for the possibility that a segmented ROI might include some pixels from the dental implant, which might in turn create outliers and an imbalanced influence on features values. Each ROI intensity values were normalized between $\mu \pm 3\sigma$ where $\mu$ was the mean value of the gray levels inside the ROI and $\sigma$ the standard deviation. The gray levels that were located outside the range $[\mu-3\sigma, \mu+3\sigma]$ were excluded from further analysis.

***Algorithm implementation***

The ROI segmentation and registration methods as well as the feature extraction computations and stepwise regression analysis were all implemented in Matlab R2012 (MathWorks, 3 Apple Hill Drive Natick, Massachusetts 01760, USA). The ROC analysis was performed with the NCSS, PASS and GESS software package (NCSS, 329 North 1000 East, Kaysville, Utah84037, USA). The computer used for processing had a Dual Core AMD 64 Athlon processor running at 2.8 GHz and 4 GB of RAM.

## Results and discussion

Regarding the dental implant boundary extraction, the proposed MRF model consists of two components: a random region labeling component (Figure 2a) which serves as the initialization step of the model and a combination of two textural features that serve as input to the model. Image gray level and local entropy values that represent textural information for each pixel were employed as input to the MRF segmentation algorithm in order to fit the image data into the two final clusters. The MRF algorithm provided as an output, a binary image presenting two final clusters (i.e., one cluster concerning the area that presents with a high x-ray reflectance (implant) and a second cluster concerning the areas in the image with a high x-ray absorbance (surrounding tissue and bone – Figure 2b). The segmented implant border it depicted in Figure 2c.

The main challenge in estimating the implant segmentation performance is "ground truth", i.e. defining implant borders. In this study an expert observer, a dentist with seventeen years of experience, has defined the ground truth by generating manual outlines of the implant. The degree of overlap between the two segmented areas, as derived by the observer–"ground truth" and the computer, was used to assess accuracy. Overlap is defined as the ratio of intersection over the union of the two segmented areas, the ground truth and the computer-generated one (33). The value of overlap is bound between zero (no overlap) and one (exact overlap). To assess the difference in the segmented border shape, mean ($d_{mean}$), root mean square ($d_{rms}$) and maximum ($d_{max}$) distance between the computer- and manually-defined borders were calculated for the 96 implants included in the dataset. The proposed implant segmentation method demonstrated a high segmentation accuracy, corresponding to overlap=0.934 ± 0.010, $d_{mean}$=2.172 ± 0.345 pixels, $d_{rms}$=3.826 ± 0.301 pixels, and $d_{max}$=7.867± 3.047 pixels.

To identify circular ROIs from bone-to-implant contact region, sampling the tissue in between and adjacent to the implant windings, the cluster corresponding to the implant boundary was subjected to morphological closing using a circular closing element of varying size (7-10 pixels), from whom the original MRF implant cluster was subtracted. This result in the area segments (Figure 2d) of the bone to implant contact region to which the circular sampling ROIs sizes were adapted (Figure 2e).

To improve ROI detection rate further, a home developed Graphical User Interface (GUI) is introduced, on top of the automated ROI identification system proposed, allowing for manual placing of circular ROIs in the bone-to-implant contact regions missed by the automated step (Figure 2f). The radiologist exploring the GUI places 2 control points one corresponding to the center of bone-to-implant contact region and the second one used to define the radius of the ROI. The application of the proposed bone-to-implant contact region identification system resulted in 573 circular ROIs of Class I and 573 ROIs of Class II (mean ROI area= 209.00 ±81.49 pixels and pixel size=23.6 μm).

The stepwise regression analysis procedure in the feature set (41 textural features) towards feature reduction was performed utilizing the threshold of probability to enter and the probability to remove 0.05 & 0.10 respectively, leading to a subset of 4 features (Angular Second Moment, Correlation, Long Run Emphasis and Gray Level Non Uniformity). Table 2 provide the results of the ROC analysis employed at both (PRP and test) groups respectively for the selected feature set. All features selected from the stepwise regression analyses procedure achieved AUC values greater than 0.77 in the PRP group, yielding increased differentiation capability for the selected features. On the contrary, in the control group the corresponding AUC values were smaller ranging from 0.56 – 0.68 (Table 2) indicating lesser osseo-integration activity in the bone-to-implant regions compared with the PRP group. The corresponding box plots of each feature from the selected subset are depicted in Figure 3.

To our knowledge the only texture-based study that investigated the bone regeneration properties in Dental implants after the PRP immersion was held by Wojtowicza et al. (17) by means of Fourier and fractal analysis. That study, considered of a very limited dataset (1 patient), and had shown that the fractal dimension feature exhibits a high performance in the bone regeneration procedure evaluation. However, in our clinical dataset this particular feature exhibited poor differentiation performance (AUC=0.57). The other aforementioned methods (13-16) studied bone remodeling in dental implants in radiographs or CT scans without the use of PRP.

Texture analysis carried out in the present study has demon-

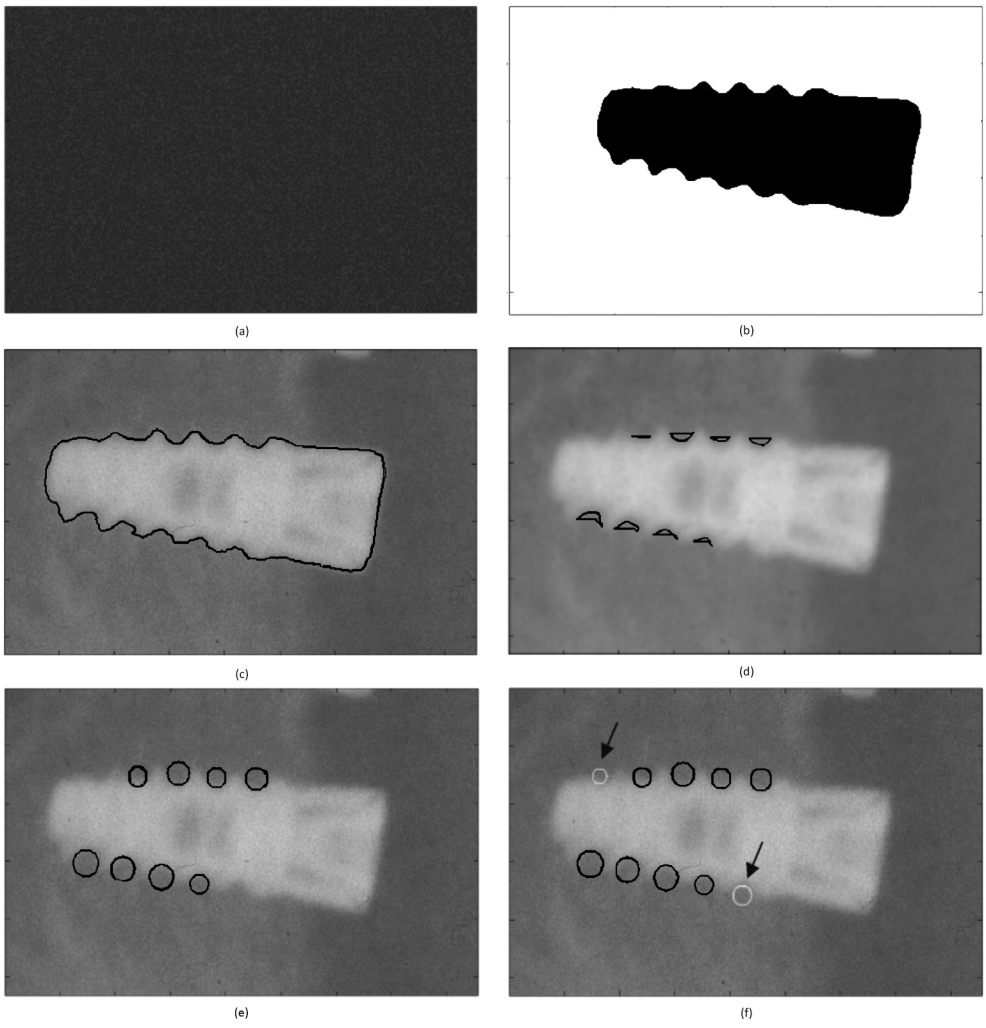


Figure 2 a, b, c, d, e, f - (a) Random image initialization, (b) MRF clusters, (c) implant segmentation (black outline), (d) areas of bone to implant contact, (e) fitted circular sampling ROIs (black color), and (f) radiologists' selected ROI (gray color).

Table 2 - Subset of textural features after Stepwise Regression analysis & ROC analysis results in the PRP & CONTROL groups.

| Textural Feature | PRP GROUP<br>AUC<br>(LOWER – UPPER 95.0% CONFIDENCE LIMIT) | CONTROL GROUP<br>AUC<br>(LOWER – UPPER 95.0% CONFIDENCE LIMIT) |
|---|---|---|
| Angular Second Moment (Average) | 0.80<br>(0,69 – 0,87) | 0.66<br>(0,55 – 0,69) |
| Correlation (Average) | 0.78<br>(0,74 – 0,82) | 0.61<br>(0,58 – 0,66) |
| Long Run Emphasis (Average) | 0.77<br>(0,68 – 0,83) | 0.56<br>(0,49 – 0,61) |
| Gray Level Non Uniformity (Range) | 0.81<br>(0.76 – 0.85) | 0.68<br>(0.59 – 0.73) |

strated a significant difference in the selected texture subset between the two groups. Regarding the PRP group, the four selected image texture features in this study are capable of capturing the increased temporal texture differentiation, compared to the control group, in the bone to implant contact regions that can be attributed to PRP effect to bone remodeling. The presented results are in total accordance with previous studies (6-8) that analyzed histological and histomorphometric data of animal and human tissue in the same contact regions. Angular Second Moment (ASM), Correlation (COR) and Gray Level Non Uniformity (GLNU) features describe the spatial dependencies, the degree of homogeneity and the presence of large run lengths within the bone-to-implant region and take high values in regions with great variability.

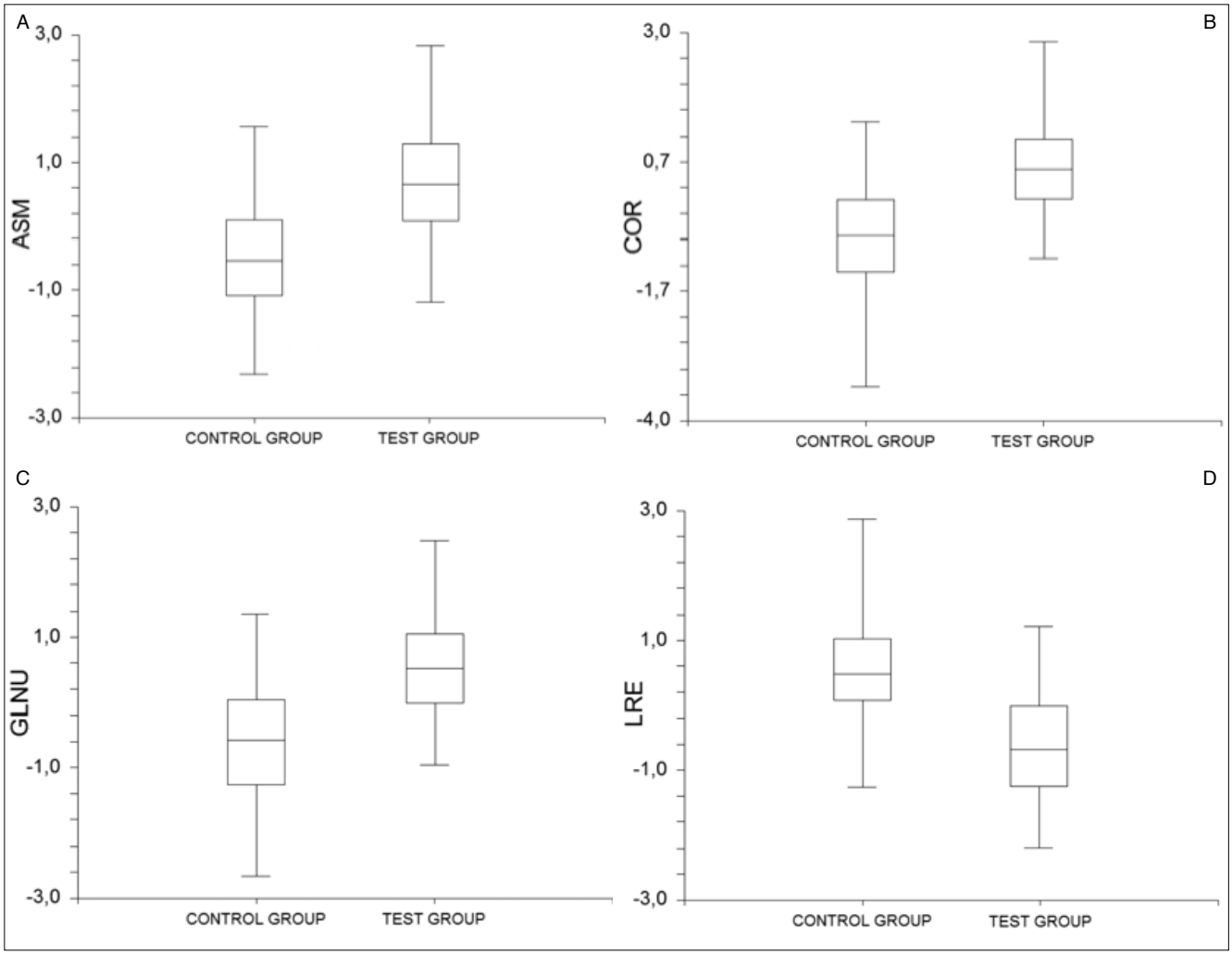


Figure 3 a, b, c, d - Box plots from the selected subset for both groups, (a) Angular Second Moment (ASM), (b) Correlation (COR), (c) Gray Level Non Uniformity (GLNU), and (d) Long Run Emphasis (LRE).

Long Run Emphasis (LRE) feature is indicative of long runs and in contrast with the other features it takes low values for areas with high variability.

All features in the selected subset from the PRP group carry the temporal alteration of the gray value profile within the bone-to-implant interface. The co-occurrence based features (Angular Second Moment and Correlation) had a tendency toward higher values in the PRP-treated cases, which in turn suggest that a newly bone-regeneration procedure is active within the implant windings. The run-length features (Long Run Emphasis and Gray Level Non Uniformity) also demonstrate the luck of the gray level uniformity during this time period which also proves the variable state of the gray values due to the osteo-regererative procedure that takes place within the bone-to-implant interface. In particular, GLNU presented relatively higher values in the cases where PRP was applied, whereas LRE presented lower values due to high variability in the bone-to-implant region (Figure 3a,b,c).

In the control group, the ASM, COR and GLNU features presented lower values compared to PRP group which in turn suggest that the osteo-regererative procedure is less active. In the same context the LRE values in control group exhibited higher values due to less variability of the gray value profile within the bone-to-implant interface (Figure 3d).

The proposed image analysis scheme attempts for the first time to contribute to the current debate, whether PRP benefits the bone regeneration or not, exploiting radiographic image appearance. The present study exploits within a clinical dataset (PRP and control group) an extended computerised feature set in dealing with image appearance differentiation between immediate implant loading (Class I) and after 8 month follow up period (Class II) representing osseointegration or not. This effect is investigated by means of the ROC analysis providing a more robust measure of differentiation.

Despite the fact that bone formation evaluation is carried out mostly in Computed Tomography dental images, it is not the first time that X-rays are employed in computerized analysis towards either bone or other structure temporal alteration. Even in a single plane (such as panoramic radiographs) the sophisticated 2nd order textural features (co-occurrence and run-length features) employed in this study have the potential to reveal any changes in the absorption of x-rays throughout time. This implies that the quantification of any absorption change could be attributed to bone density alteration. We strongly believe that this study could provide new knowledge regarding the debate around PRP.

The outcome of the proposed method is of a significant clinical interest because it reinforces the prevailing view of the dental community, that PRP augments the osteo-regenerative potential of surrounding tissues after dental implanting, which in turn orients the daily surgical procedure towards PRP employment.

## Conclusion

The temporal texture differentiation associated with the bone regeneration properties, around loaded oral implants, after Platelets Rich Plasma (PRP) application, was investigated in a follow up clinical sample of panoramic radiographs by means of the differentiation of the image texture. The results of the ROC analysis demonstrated that the addition of PRP had a significantly positive effect on bone formation as captured by dental panoramic radiographs.
In terms of analyzing the information in widely used panoramic radiographs, the proposed approach in PRP effect quantification and evaluation, highlights the potential of appropriately designed image analysis methods, such as segmentation and texture analysis, as essential auxiliary tools, in an image based tissue parameterization and quantification.

**Conflict of interest**. The Authors declare that there is no conflict of interests regarding the publication of this article.

## References


1. Natali AN. Dental Biomechanics. London/New York: Taylor & Francis, 2003:69-87.
2. Esposito M, Grusovin MG, Willings M, Coulthard P, Worthington HV. The effectiveness of immediate, early, and conventional loading of dental implants: a Cochrane systematic review of randomized controlled clinical trials. Int J of Oral &Maxillofac Implants. 2007:22(6):893-900.
3. Kengo Shimono, Masamitsu Oshima, Hikaru Arakawa, Aya Kimura, Kumiko Nawachi, Takuo Kuboki. The effect of growth factors for bone augmentation to enable dental implant placement: A systematic review Japanese Dental Science Review. 2010:46(1):43-53.
4. Zechner S, Tangi G, Tepper S, Furst G, Bernhart T, Haas R, Mailath G, Watzek G. Influence of Platetel-rich Plasma on Osseus Healing of Dental Implants: A Histologic and Histomorphometric Study in Minipigs. Int J Oral Maxillofac Implants. 2003:18(1):15-22.
5. Terheyden H, Roldan-Ossa JC, Miller J, Jepsen S, Acil Y. Platelet-rich plasma in bone regeneration. Preliminary results of two experimental studies. Implantologie. 2002:10:195-205.
6. Garg AK. The use of platelet rich plasma to enhance the success of bone grafts around dental implants. Dent Implantol Update. 2000:11(3):17-21.
7. Adler SC, Kent KJ. Enhancing wound healing with growth factors. Facial Plast Surg Clin North Am. 2002:10(2):129-146.
8. Kim SG, Chung CH, Kim YK, Park JC, Lim SC. Use of particulate dentin-plaster of Paris combination with/without platelet rich plasma in the treatment of bone defects around implants. Int J Oral Maxillofac Implants. 2002:17 (1):86-94.
9. Froum SJ, Wallace SS, Tarnow DP, Cho SC. Effect of platelet rich plasma on bone growth and osseointegration in human maxillary sinus grafts: Three bilateral case reports. Int J Periodontics Restorative Dent. 2002:22(1):45-53.
10. Shanaman R, Filstein MR, Danesh-Meyer MJ. Localized ridge augmentation using GBR and platelet-rich plasma: case reports. Int J Periodontics Restorative Dent. 2001:21(4):345-55.
11. DohanEhrenfest DM, Rasmusson L, Albrektsson T. Classification of platelet concentrates: from pure platelet-rich plasma (P-PRP) to leucocyte- and platelet-rich fibrin (L-PRF). Trends Biotechnol. 2009:27(3):158-67.
12. Trisi P. Why Science? Why Research?. Implant Dentistry. 2008:17(4):373-374.
13. Gatti M, Poli G. Image analysis of dental implants. Journal of Biomechanics. 1985:18(7):519.
14. Youssif A, Chowdhury MU, Ray S. Computer Aided Analysis of Dental Radiographic Images. In Proceedings of the Digital Image Computing: Techniques and Applications. 2005:43-48.
15. Barone A, Covani U, Cornelini R, Gherlone E. Radiographic bone density around immediately loaded oral implants. Clin Oral Implants Res. 2003:14(5):610-615.
16. Wilding RJC, Slabbert JCG, Kathree H, Owen CP, Crombie K, Delport P. The use of fractal analysis to reveal remodelling in human alveolar bone following the placement of dental implants. Archives of Oral Biology. 1995:40(1):61-72.
17. Wojtowicza A, Chaberekb S, Krysta L, Urbanowskac E, Ciechowicza K, Ostrowskid K. Fourier and fractal analysis of maxillary alveolar ridge repair using platelet rich plasma (PRP) and inorganic bovine bone. Int J of Oral and Maxillofacial Surgery. 2003:32(1):84-86.
18. Tae-Min Y, Byung-Ho C, Shi-Jiang Z, Jae-Hyung J, Seoung-Ho L, Jin-Young H, Hyun-Jung L, Jingxu L. Platelet-enriched fibrin glue and platelet-rich plasma in the repair of bone defects adjacent to titanium dental implants. Int J of Oral and Maxillofacial Surgery. 2007:22(3):417-22.
19. Griffin TJ, Cheung WS. Treatment of gingival recession with a platelet concentrate graft: a report of two cases. Int J Periodontics Restorative Dent. 2004:24(6):589-595.
20. European Commission. European Guidelines on Radiation Protection in Dental Radiology. Luxembourg: RP 136, 2004.
21. Efstathopoulos EP, Costaridou L, Kocsis O, Panayiotakis G. A protocol-based evaluation of medical image digitizers. Br J Radiol. 2001:74(885):841-6 74.
22. Besag JE. Spatial interaction and the statistical analysis of lattice systems. J R Stat Soc Ser B 1974;36:192-236.
23. Geman S, Geman D. Stochastic relaxation, Gibbs distributions, and the Bayesian restoration of images. IEEE. Trans. Pattern. Anal. Mach.Intell. 1984;6:721-741.
24. Kirkpatrick S, Gelatt CD, Jr., Vecchi MP. Optimization by simulated annealing. Science 1983;220:671-680.
25. Haralick R, Shanmugam K, Dinstein I. Textural features for image classification. IEEE Transactions on Systems Man and Cybernetics. 1973:3:610-621.
26. Galloway MM. Texture Analysis Using Gray Level Run Lengths. Computer Graphics and Image Processing 1975:4:172-179.
27. Liu JZ, Zhang LD, Yue GH. Fractal Dimension in Human Cerebellum Measured by Magnetic Resonance Imaging. Biophysical Journal. 2003:85:4041-4046.
28. Draper NR, Smith H. Applied Regression Analysis. Hoboken, NJ: Wiley-Interscience, 1998.
29. Peng HC, Long F, Ding C. Feature selection based on mutual information: criteria of max-dependency, max-relevance, and min-redundancy. IEEE Transactions on Pattern Analysis and Machine Intelligence 2005;27(8):1226-1238.
30. Huang K, Velliste M, Murphy RF. Feature reduction for improved recognition of subcellular location patterns in fluorescence microscope images. Proceedings of SPIE 2003:307-318.
31. Fawcett T. An introduction to ROC analysis. Pattern Recognition Letters 2006:27:861-874.
32. Lasko TA, Bhagwat JG, Zou KH, Ohno-Machado L. The use of receiver operating characteristic curves in biomedical informatics. Journal of Biomedical Informatics. 2005:38:404-415.
33. Kupinski MA, Giger ML. Automated seeded lesion segmentation on digital mammograms. IEEE Trans. Med. Imaging. 1998;17:510-517.